

Magnetic Properties of the Heusler Ru₂MnX (X = Nb, Ta or V) Compounds: Monte Carlo Simulations

N. Saber, Z. Fadil, A. Mhirech, B. Kabouchi, L. Bahmad* and W. Ousi Benomar

Laboratoire de Matière Condensée et Sciences Interdisciplinaires (LaMCSi), Faculty of Sciences. P.O. Box 1014, Mohammed V University in Rabat, Morocco

Abstract:

In this paper, we have focused on a comparison of the different magnetic properties of the three nano-Heusler Ru₂MnX (X = Nb, Ta or V) compounds using the Blume-Capel Ising model. The Heusler structures are composed by different mixed spins. In fact, the Ru and Mn atoms are modeled by spin-5/2 and spin-1/2, respectively. While, the X atoms (X = Nb, Ta and V) are represented by the spin-7/2, spin-3/2 and spin-5/2, respectively.

This study is carried out by using the Monte Carlo simulations under the Metropolis algorithm. The magnetic behaviors of the three nano-Heusler compounds have been studied and discussed. It is found that Ferrimagnetic to superparamagnetic transitions were observed corresponding to different blocking temperatures. Besides, the effect of the crystal field, the exchange coupling interactions and the external magnetic field have been inspected on the magnetization of each nano-Heusler compound Ru₂MnX (X = Nb, Ta or V).

Keywords: Nano-Heusler compounds; Magnetic properties; Monte Carlo simulations; Superparamagnetic phase; Blocking temperature; Magnetic hysteresis cycles.

*) Corresponding author: bahmad@fsr.ac.ma (L. B.)

1. Introduction:

Heusler alloys [1,2] have become one of the important groups of materials for rapidly growing technology due to their application [3-10]. These materials are often used in spintronics, shape memory alloys, magnetocaloric materials and many others [11]. Frequently, Heusler alloys can be classified into four main groups as alloys of full Heusler, half Heusler, reverse Heusler and quaternary Heusler [11]. These Heusler alloy groups have received great interest especially through theoretical work [12-17]. Moreover, Monte Carlo simulations (MCS) have made it possible to study the magnetic or dielectric properties of different structures by determining and varying the transition temperature in Ising ladder-like graphene nanoribbon [18], bilayer graphene-like structure [19], borophene layers structure with RKKY interactions [20], bi-layer graphyne-like structure [21], monolayer coronene-like nano-structure [22], monolayer nano-graphyne structure [23], diamond-like decorated square [24] and in decorated triangular lattice [25]. The MCS are also used to investigate the compensation temperature, in spin-1/2 Ising trilayer [26], trilayer graphyne-like [27], monolayer naphthalene-like nanoisland [28], borophene core-shell [29], ovalene [30] and in nano-trilayer graphene [31]. Indeed, MCS leads to interesting results and allows a better understanding of the nanostructures by varying different physical parameters. Furthermore, the MCS has been used to investigate the magnetic properties of the different Heusler compounds in Co-Fe-Mn-Si [32], Ni-Mn-Ga [33], Ni-Mn-Ga-Cr [34] and magnetocaloric effect in $\text{Ni}_{50}\text{Mn}_{34}\text{In}_{16}$ [35]. In some our earlier works, we have studied and discussed the different properties of the different Heusler structures [36-39].

In the present work, we study the magnetic properties of Heusler compounds Ru_2MnX ($X = \text{Nb}, \text{Ta}$ or V). Indeed, we aim is to compare the behavior magnetic properties in these three Heusler compounds. The investigated system is explored using the well-known Monte Carlo simulations under the Metropolis algorithm. As far as we know, there are no theoretical investigations in the literature that have studied the magnetic properties of Heusler compounds Ru_2MnX ($X = \text{Nb}, \text{Ta}$ or V). This paper is organized as follows: the model and method used are illustrated in section 2, the numerical results and discussion are reported in section 3. Finally, a conclusion is given in section 4.

2. Model and method:

In this work, we study the magnetic properties of nano-Heusler structures Ru_2MnX composed with three types of atoms: Ruthenium, Manganese and X. In our case, we study the nano-Heusler structure by replacing X atom with three types of atoms: titanium, vanadium and niobium ($X=\text{Ta}, \text{V}$ or Nb), respectively.

In this work, the total number of each atom is as follows: $N_{\text{Ru}}=123$, $N_{\text{Mn}}=32$ and $N_{X=\text{Ta}, \text{V}, \text{Nb}}=32$ (see Fig. 1). Besides, such nano-Heusler structures are studied using the Blume Capel model with free boundary conditions. Additionally, our data were generated with 10^6 Monte Carlo steps per spin, we neglect the 10^5 first Monte Carlo steps of the simulations to balancing the system.

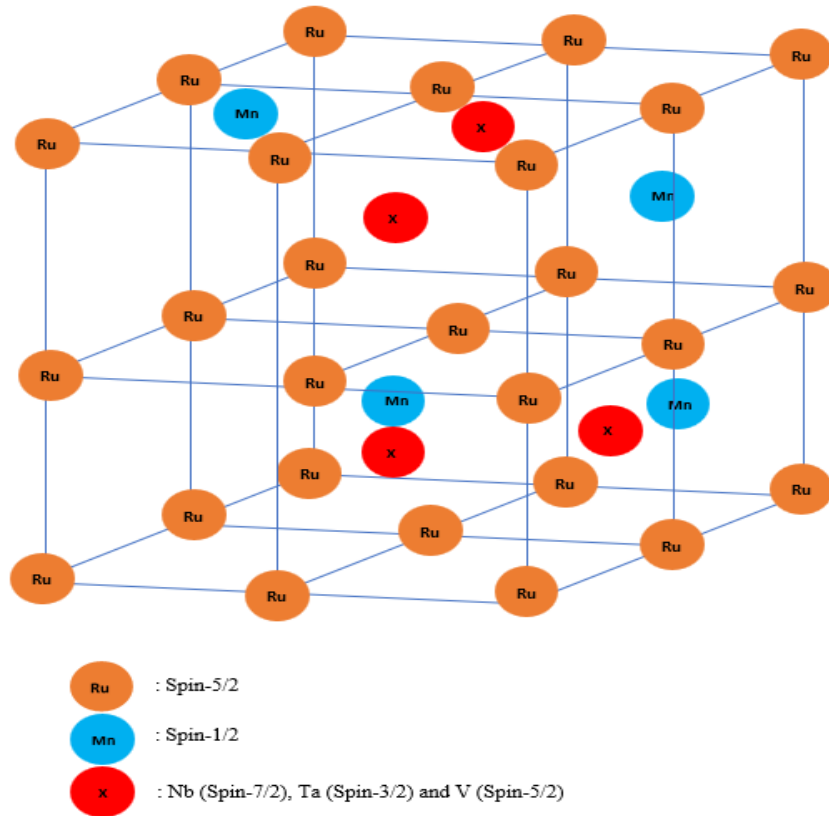


Fig. 1: A schematic representation of Heusler structure Ru_2MnX ($X=\text{Ta}, \text{V}$ or Nb), Ru with spin-5/2 (orange balls), Mn with spin-1/2 (blue balls), Ta with spin-7/2, V with spin-3/2 and Nb with spin-5/2 (red balls).

The Hamiltonian of Heusler structure is defined as:

$$\begin{aligned} \mathcal{H} = & -J_{\text{Ru Mn}} \sum_{\langle i,j \rangle} \text{Ru}_i \text{Mn}_j - J_{\text{Ru X}} \sum_{\langle i,k \rangle} \text{Ru}_i \text{X}_k - H \sum_i (\text{Ru} + \text{Mn} + \text{X}) \\ & - D_{\text{Ru}} \sum_i \text{Ru}_i^2 - D_{\text{X}} \sum_k \text{X}_k^2 \end{aligned} \quad (1)$$

where $J_{\text{Ru Mn}}$ and $J_{\text{Ru X}}$ represents the exchange coupling interactions between two first nearest neighbor atoms with spins Ru – Mn, Ru – X (X=Ta, V or Nb), respectively.

H is the external magnetic field. The crystal fields D_{Ru} and D_{X} are acting on the spin atoms of Ru and X, respectively. In all this work, we will take the identical crystal fields acting on the spins Ru and X: $D=D_{\text{Ru}}=D_{\text{X}}$.

The internal energy per site of the studied Heusler structure is:

$$E = \frac{1}{N_{\text{T}}} \langle \mathcal{H} \rangle \quad (2)$$

With: $N_{\text{T}} = N_{\text{Ru}} + N_{\text{Mn}} + N_{\text{X=Ta, V, Nb}} = 123+32+32=187$ atoms

The corresponding partial and total magnetizations are:

$$M_{\text{Ru}} = \frac{1}{N_{\text{Ru}}} \sum_i \text{Ru}_i \quad (3)$$

$$M_{\text{Mn}} = \frac{1}{N_{\text{Mn}}} \sum_j \text{Mn}_j \quad (4)$$

$$M_{\text{X}} = \frac{1}{N_{\text{X}}} \sum_k \text{X}_k \quad (5)$$

With $N_{\text{X}} = N_{\text{Ta}} = N_{\text{V}} = N_{\text{Nb}}$

$$M_{\text{tot}} = \frac{N_{\text{Ru}} M_{\text{Ru}} + N_{\text{Mn}} M_{\text{Mn}} + N_{\text{X}} M_{\text{X}}}{N_{\text{Ru}} + N_{\text{Mn}} + N_{\text{X}}} \quad (6)$$

3. Numerical results and discussion

In this section, we study the magnetic properties of three nano-Heusler structures Ru_2MnX ($X=\text{Ta}$, V or Nb) using Monte Carlo simulations under the Metropolis algorithm.

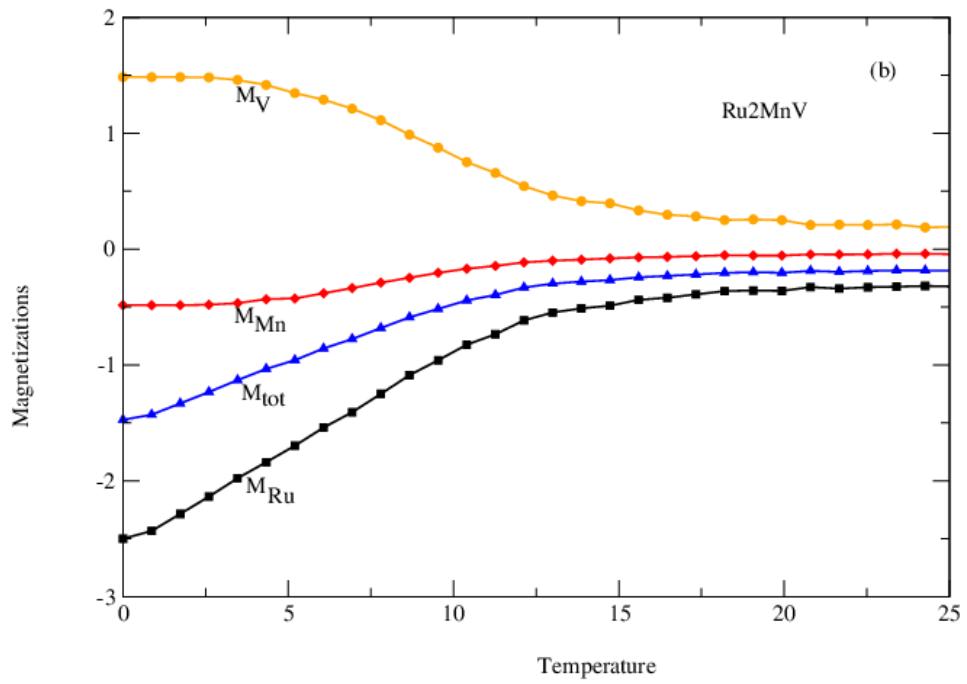
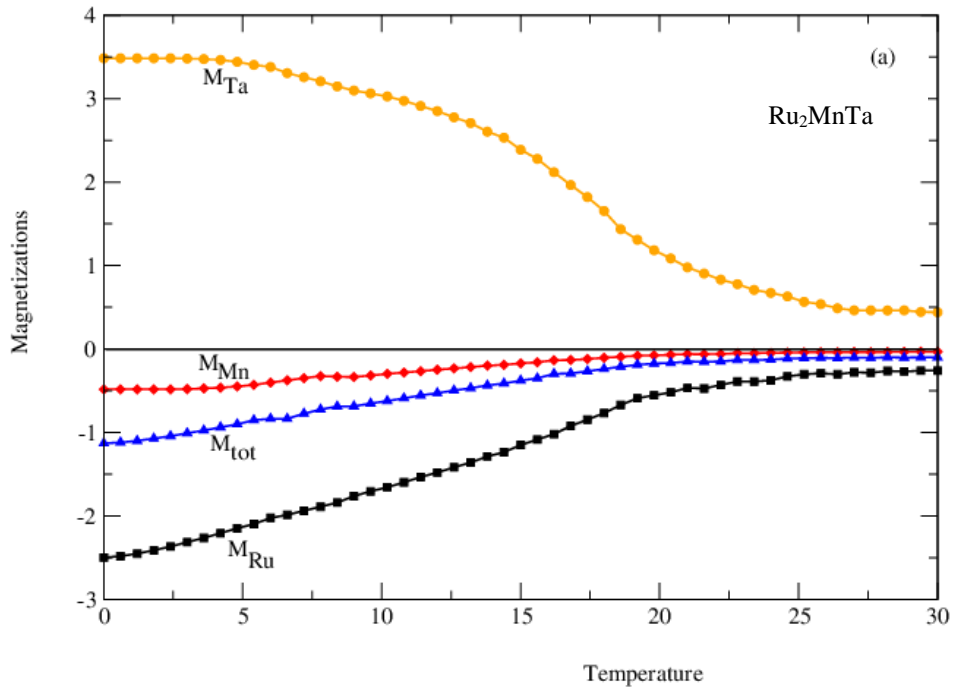
In Fig. 2a, 2b and 2c, we illustrate the magnetizations of different nano-Heusler structures as a function of the temperature: Ru_2MnTa , Ru_2MnV and Ru_2MnNb , respectively. These figures are plotted in the absence of the crystal and external magnetic fields ($D=0$ and $H=0$) and for fixed exchange coupling interactions: $J_{\text{Ru-Mn}} = 1$ and $J_{\text{Ru-X}} = -1$.

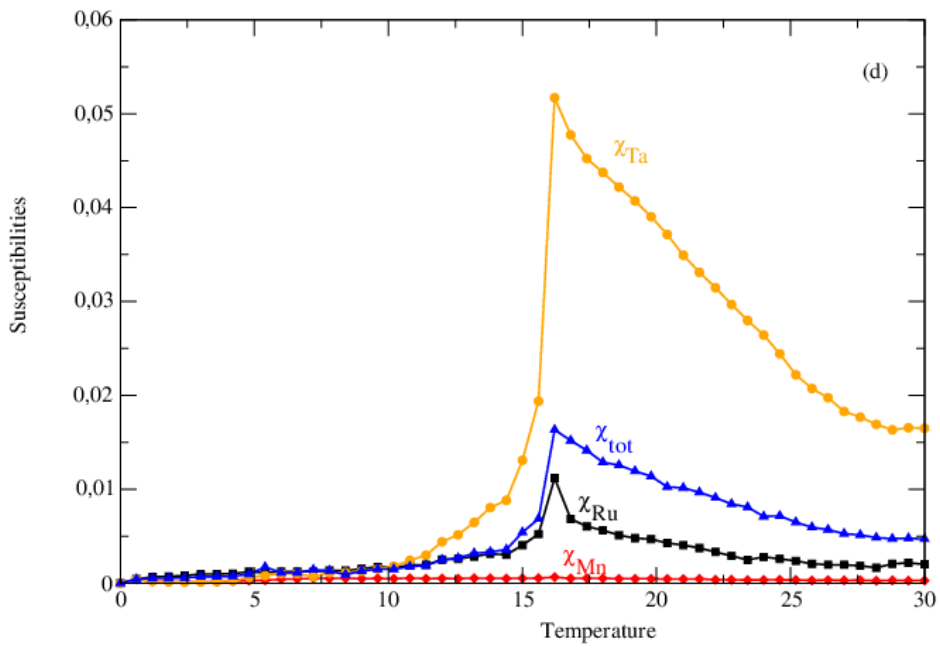
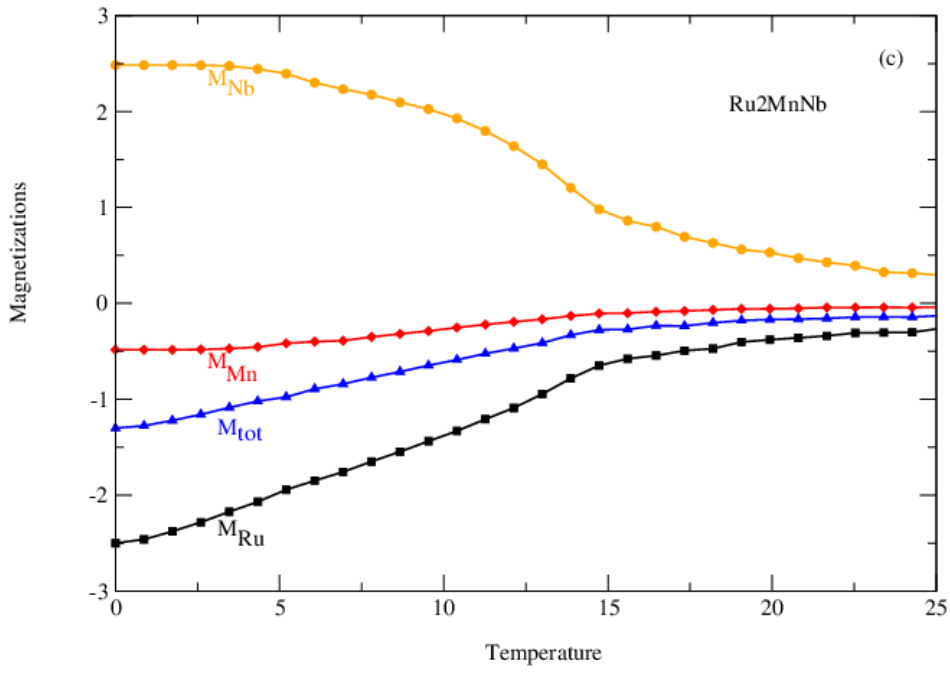
The magnetizations at very low temperature ($t \approx 0$) are $M_{\text{Ru}} = -5/2$, $M_{\text{Mn}} = -1/2$, $M_{\text{Ta}} = +7/2$, $M_{\text{V}} = +3/2$ and $M_{\text{Nb}} = +5/2$ leading to $M_{\text{tot}} = \frac{123 \times (-5/2) + 32 \times (-1/2) + 32 \times (+7/2)}{(123+32+32)} = -0.5$ for

Ru_2MnTa , $M_{\text{tot}} = \frac{123 \times (-5/2) + 32 \times (-1/2) + 32 \times (+3/2)}{(123+32+32)} = -1.3$ for Ru_2MnV and $M_{\text{tot}} =$

$\frac{123 \times (-5/2) + 32 \times (-1/2) + 32 \times (+5/2)}{(123+32+32)} = -0.5$ for Ru_2MnNb .

Moreover, in Figs. 2a, 2b and 2c, the total magnetizations of Ru_2MnTa , Ru_2MnV and Ru_2MnNb systems are in the ferrimagnetic phase where the temperature of these systems is lower than the blocking temperature ($T < T_B$), then the magnetizations increase when increasing the temperature values to reach the superparamagnetic phase ($T > T_B$). Additionally, to confirm this result and find the exact value of the blocking temperature which determines the transition between the ferrimagnetic and superparamagnetic phase, we have plotted in Fig. 2d, 2e and 2f, the total susceptibilities of the three studied systems. Indeed, the blocking temperatures of the studied systems are located at the peaks of the total susceptibilities $T_B \approx 16.25$, 12.5 and 15 for Ru_2MnTa , Ru_2MnV and Ru_2MnNb , respectively.





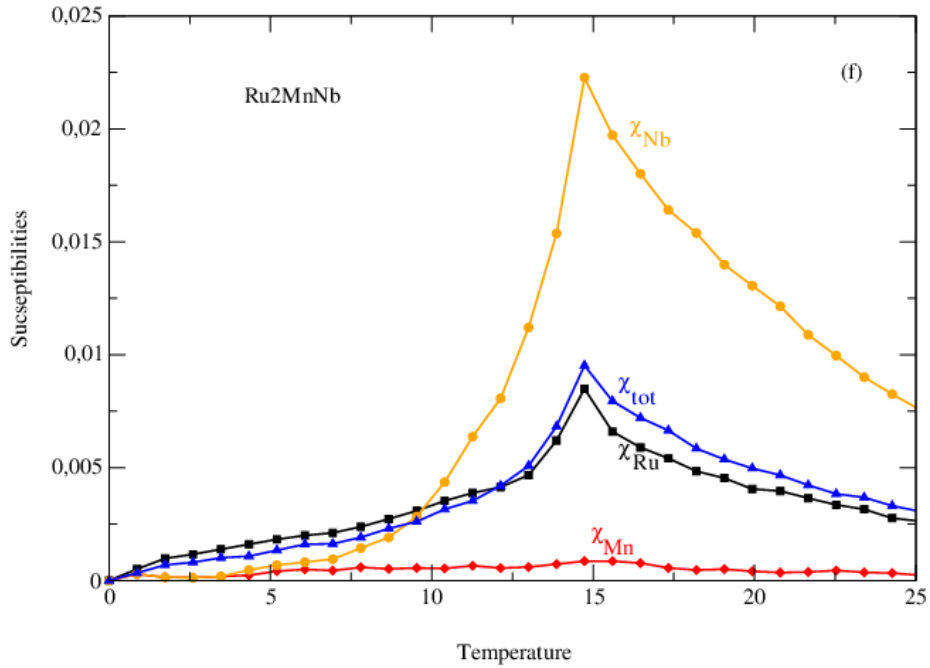
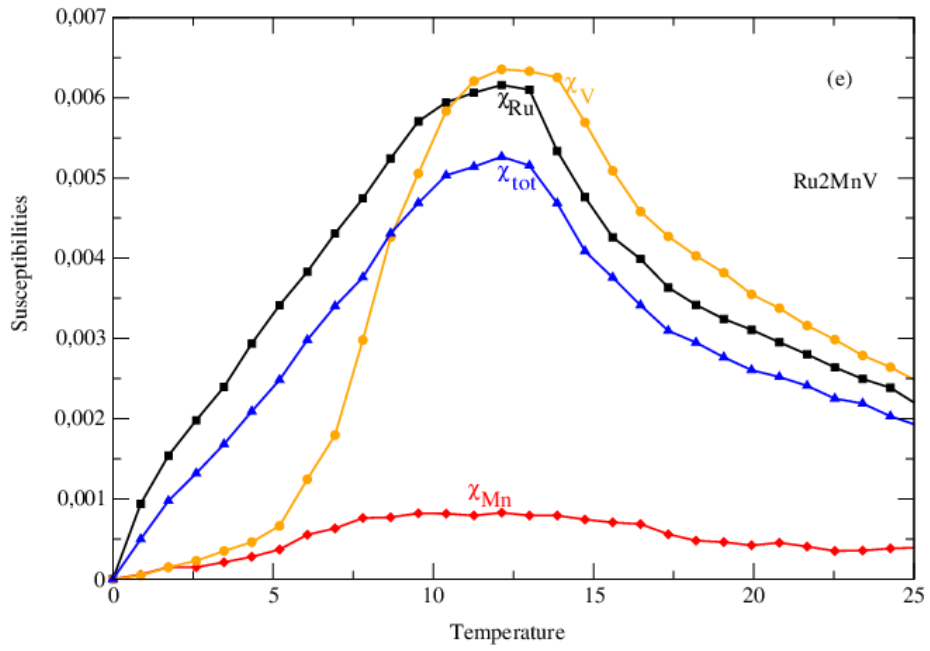
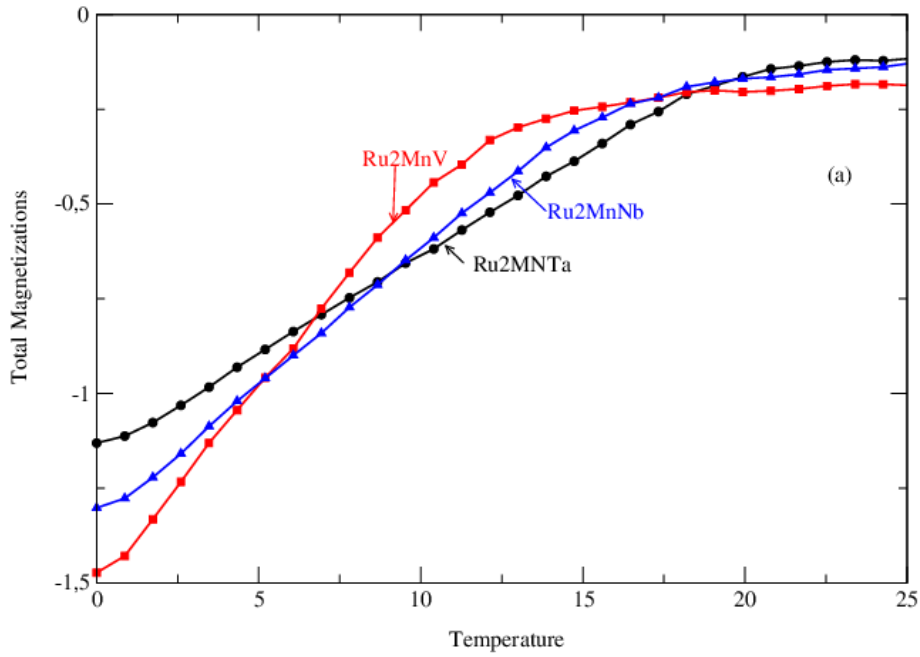


Fig. 2: Magnetizations (a, b, c) and susceptibilities (d, e, f) as a function of temperature for fixed parameter values: $H=0$, $D=0$, $J_{Ru-Mn} = 1$ and $J_{Ru-X} = -1$.

In Fig. 3a, we examine the variation of the thermal magnetization in different nano-Heusler components (Ru_2MnTa , Ru_2MnV and Ru_2MnNb). This figure is plotted in the absence of the crystal ($D=0$) and external magnetic ($H=0$) fields and for the fixed exchange coupling interactions: $J_{\text{Ru-Mn}} = 1$ (ferrimagnetic case) and $J_{\text{Ru-X}} = -1$ (anti-ferrimagnetic case). From Fig. 3a, when increasing the temperature values, the total magnetization appears firstly for the Ru_2MnV compound followed by the Ru_2MnNb compound and finally for the Ru_2MnTa one. This means that Ru_2MnV compound reaches the superparamagnetic phase earlier than Ru_2MnNb compound and ultimately followed by the Ru_2MnTa one. To deduce the blocking temperature (T_B) value for each Heusler compounds, we plot in Fig. 3b the thermal susceptibility for the same parameters as in Fig. 3a. The obtained blocking temperature for the Ru_2MnV , Ru_2MnNb and Ru_2MnTa compounds are $T_B \approx 11, 15$ and 18 , respectively.



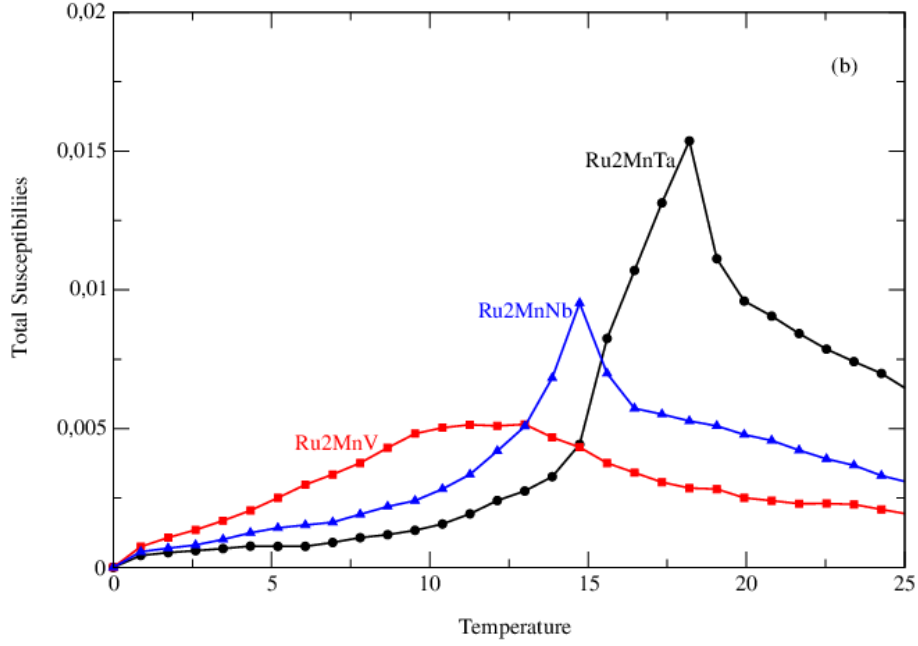


Fig. 3: Total magnetizations (a) and total susceptibilities (b) as a function of temperature for fixed parameter values: $H=0$, $D=0$, $J_{\text{Ru-Mn}} = 1$ and $J_{\text{Ru-X}} = -1$.

Following the same motivation, we explore in Fig.4a and 4b, the variation of the thermal magnetization in different nano-Heusler components. These figures are plotted in the absence of both fields ($H=0$ and $D=0$) and for the fixed ferromagnetic exchange coupling: $J_{\text{Ru-Mn}} = 1$ and $J_{\text{Ru-X}} = 1$. The blocking temperature for the Ru_2MnV , Ru_2MnNb and Ru_2MnTa compounds are $T_B \approx 12$, 17.5 and 20 , respectively. The super-paramagnetic phase is observed as the first one for Ru_2MnV compound when ($T > T_B \approx 12$) then for Ru_2MnNb compound when ($T > T_B \approx 17.5$) and finally for Ru_2MnTa one when ($T > T_B \approx 20$). Indeed, the difference between this result and that of Figs. 3a and 3b, is that when increasing the exchange coupling interaction ($J_{\text{Ru-X}}$) value, the blocking temperature also tends to increase, which means that the super-paramagnetic phase appears only for large temperature values.

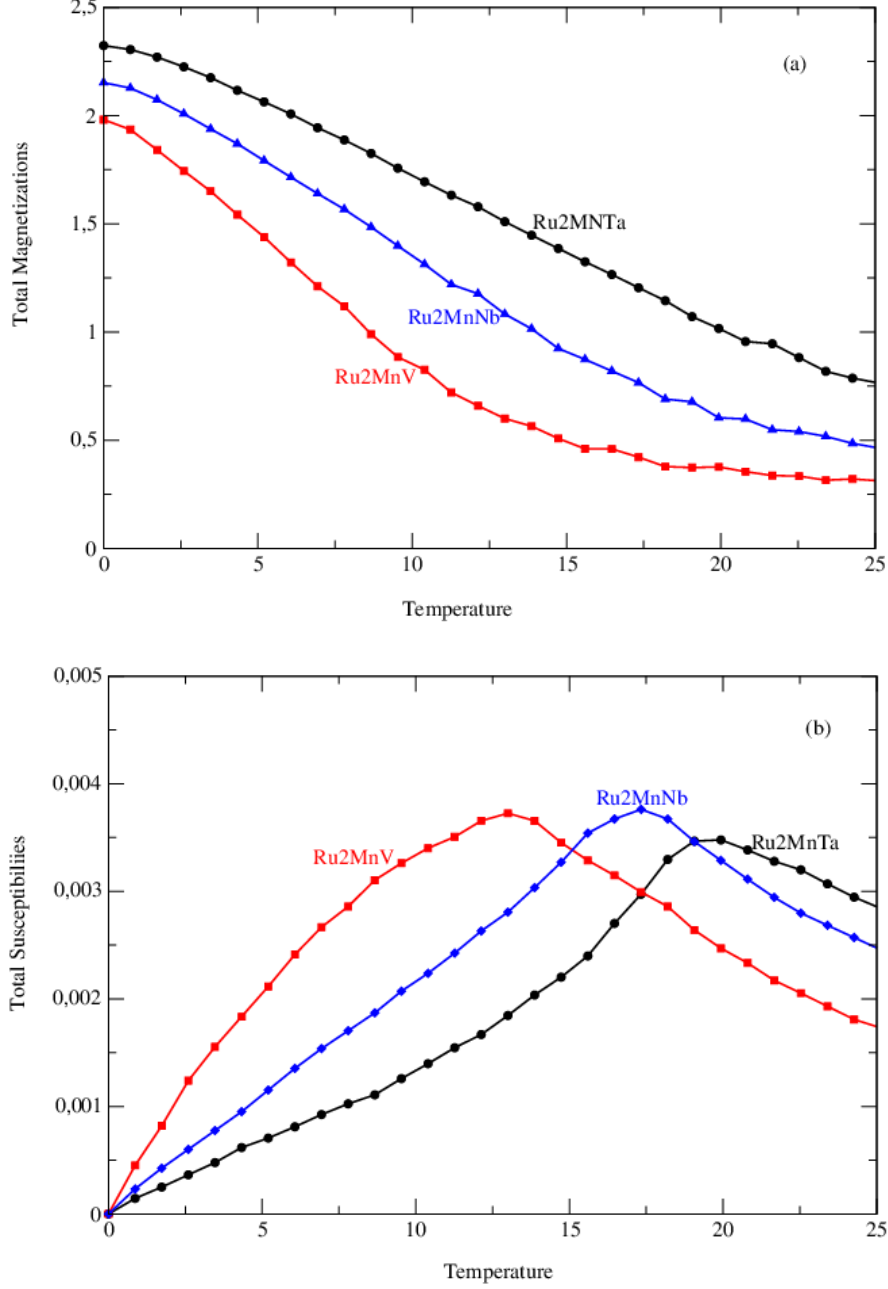
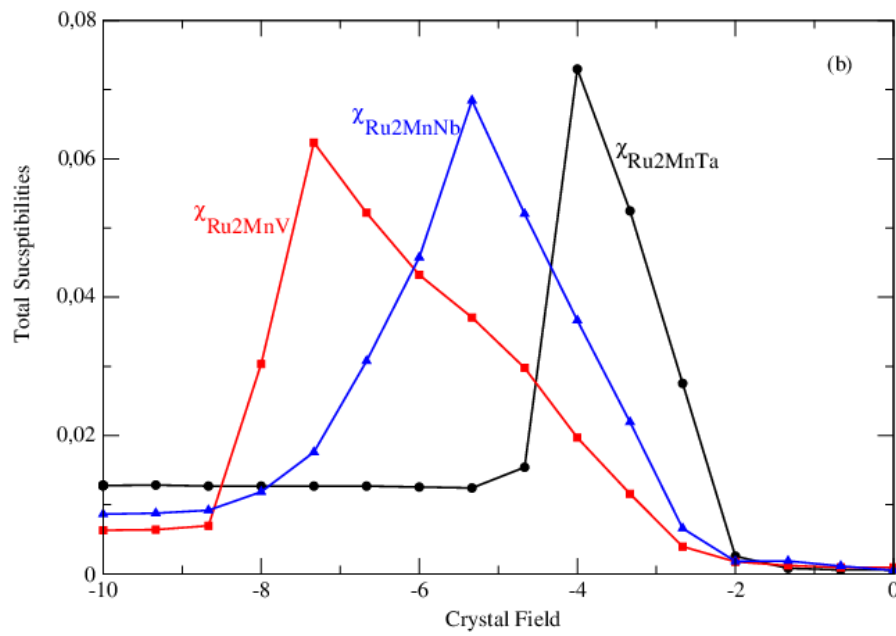
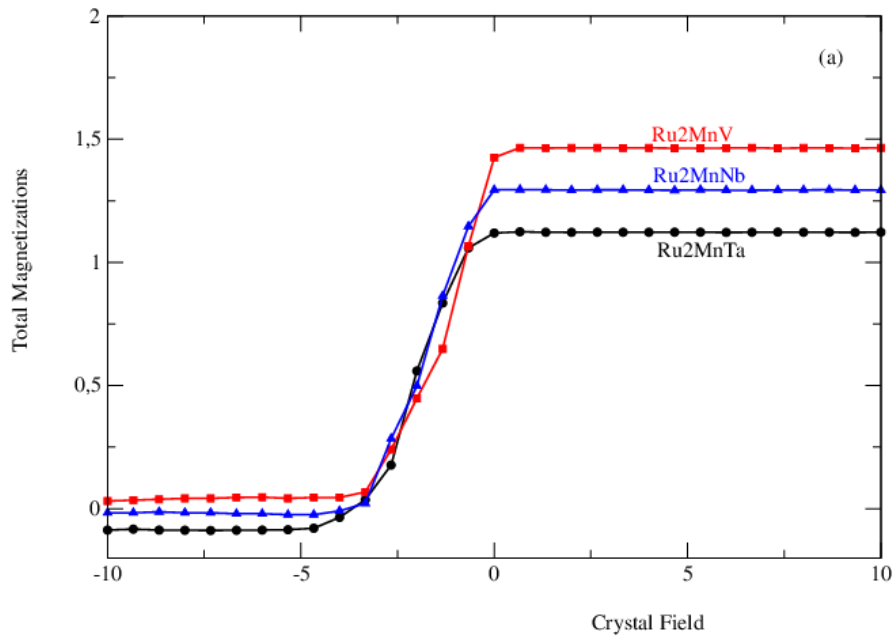


Fig. 4: Total magnetizations (a) and total susceptibilities (b) as a function of temperature for fixed parameter values: $H=0$, $D=0$, $J_{\text{Ru-Mn}} = 1$ and $J_{\text{Ru-X}} = 1$.

Besides, we present in the Figs. 5(a-d), the behavior of the total magnetizations and total susceptibilities as a function of the crystal field. Such figures are plotted for the three nan-Heusler compounds (Ru₂MnV, Ru₂MnNb and Ru₂MnTa) in the absence of the reduced external magnetic field ($H=0$) and fixed parameter values of temperature $T=1$ and exchange coupling parameter $J_{\text{Ru-Mn}} = 1$ and by changing the exchange coupling interaction between Ru and X atoms: $J_{\text{Ru-X}} = -1$ for (a, b), $J_{\text{Ru-X}} = 1$ for (c, d).

From Fig.5a, the total magnetizations of the three nano-Heusler compounds undergo a first order transition corresponding to the critical crystal field (D_T) values obtained by the susceptibility peaks in Fig. 5b. The obtained critical crystal field for Ru_2MnV , Ru_2MnNb and Ru_2MnTa compounds are $D_T \approx -7.5$, -5.5 and -4 , respectively. Then, the total magnetization of these three Heusler compounds is saturated for $D > 0$. In Fig.5c, when increasing the exchange coupling interaction ($J_{\text{Ru-X}}$) value, the total magnetizations of the three nano-Heusler compounds undergo a second order transition corresponding to the critical crystal field values given by the susceptibility peaks exposed in Fig. 5d. The obtained critical crystal field for Ru_2MnNb , Ru_2MnTa and Ru_2MnV compounds are $D_T \approx -6$, -4 and -2.5 , respectively. Afterward, the total magnetization of these three Heusler compounds is saturated for $D > 1$.



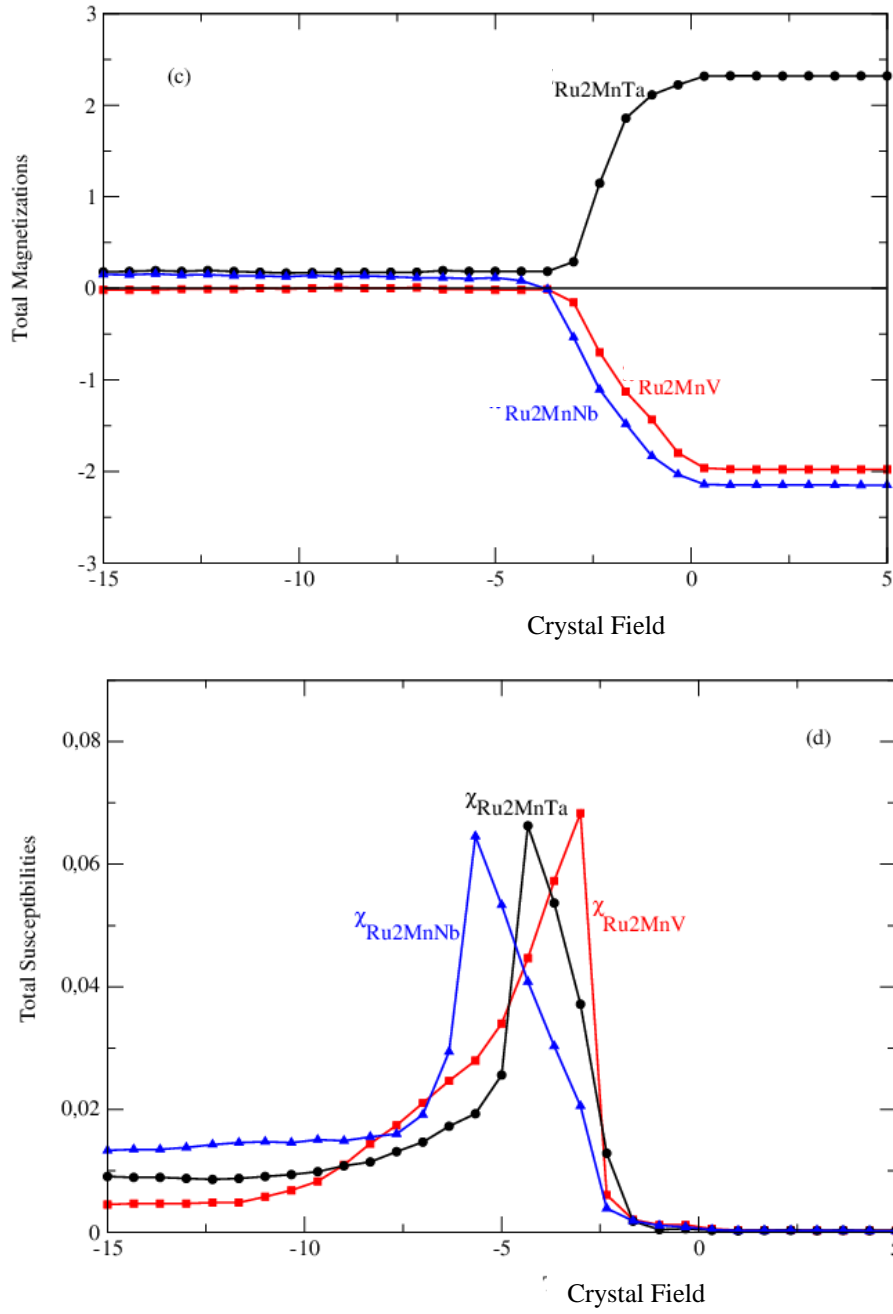
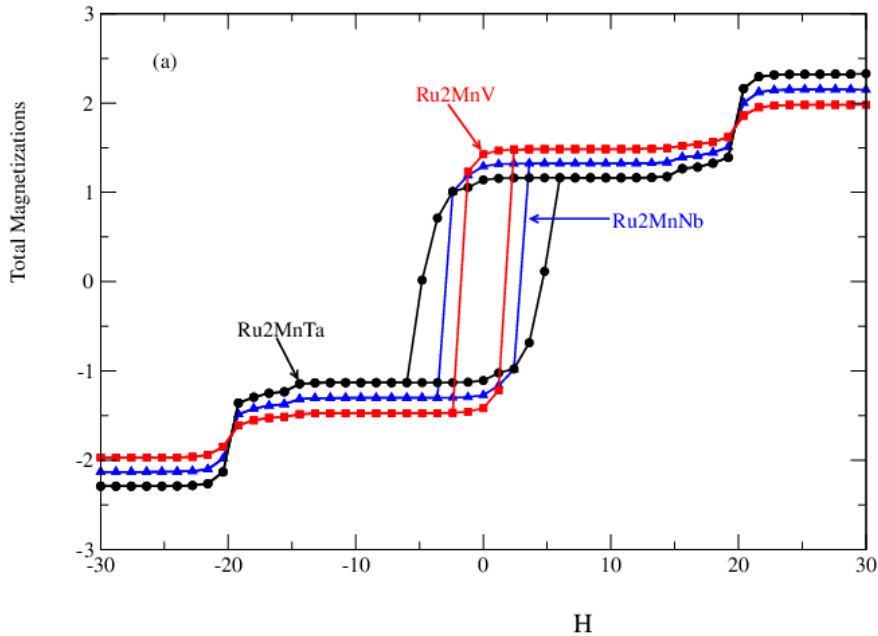


Fig. 5: Total magnetizations and total susceptibilities as a function of crystal field for fixed parameter values: $H=0$, $T=1$ and $J_{\text{Ru-Mn}} = 1$; $J_{\text{Ru-X}} = -1$ for (a, b), $J_{\text{Ru-X}} = 1$ for (c,d).

Finally, we explore in Figs.6a and 6b the magnetic hysteresis cycle behaviors of the three nano-Heusler compounds. These Figures are plotted in the absence of crystal field ($D=0$) and for a fixed temperature $T=1$: Fig. 6a is plotted for $J_{\text{Ru-X}} = -1$ (anti-ferrimagnetic case), while Fig. 6b is illustrated for $J_{\text{Ru-X}} = 1$ (ferrimagnetic case). In Fig.6a, the surface of the loops is important in the Ru_2MnTa compound followed by that of the Ru_2MnNb compound then by that of the Ru_2MnV structure. The obtained coercive field for the Ru_2MnTa , Ru_2MnNb and Ru_2MnV compounds are $H_C \approx 5, 2.5$ and 1 , respectively. The decrease in the coercive field and the surface of the loops is due to the difference in the number of atoms and spins from one nano-Heusler compound to another. Furthermore, the behavior of the total magnetization of the nano-Heusler compounds in Fig.3a confirms this result. Moreover, following the same motivation, we present Fig.6b. From this figure, when increasing the exchange coupling parameter $J_{\text{Ru-X}}$, the coercive field and the surface of the loops also tends to increase. This behavior confirms the result already found in Fig4a.



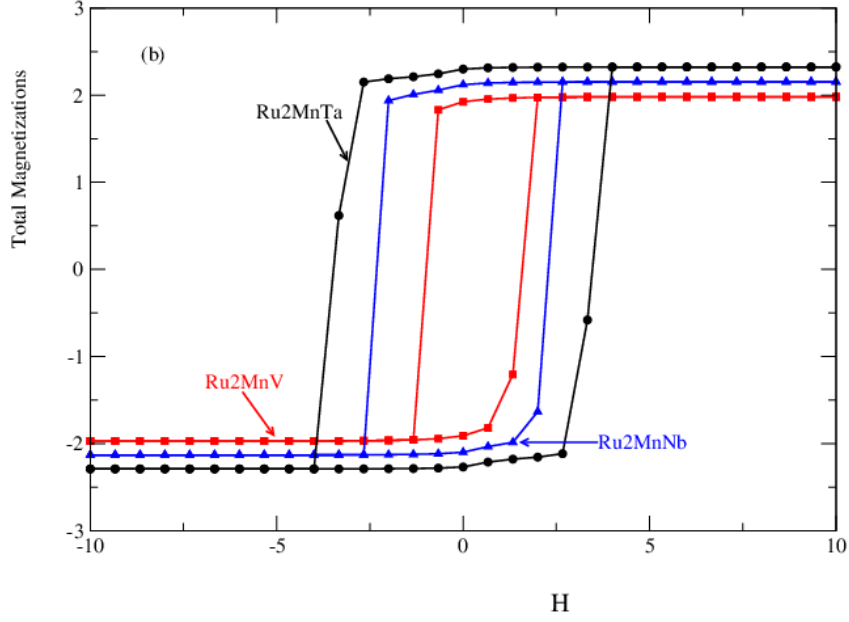


Fig. 6: Hysteresis cycles for different Heusler structure for fixed parameter values: $D=0$, $T=1$: $J_{Ru-X} = -1$ for (a), $J_{Ru-X} = 1$ for (b).

4. Conclusion

In summary, the magnetic properties, including the magnetizations, the susceptibilities, and the blocking temperature T_B , of a three nano-Heusler compounds Ru_2MnX ($X = Nb$, Ta or V) have been studied, using Blume-Capel Ising model using the Monte Carlo simulations. The Ru and Mn atoms are modeled by spin-5/2 and spin-1/2, respectively. While, the X atoms ($X = Nb$, Ta and V) are represented by the spin-7/2, spin-3/2 and spin-5/2, respectively.

It is found that Ru_2MnV compound reaches the super-paramagnetic phase earlier than Ru_2MnNb compound and ultimately followed by the Ru_2MnTa one. In fact, when increasing the exchange coupling interaction J_{Ru-X} value, the blocking temperature increase which mean that the super-paramagnetic phase appears for larger temperature values. Besides, corresponding to the critical crystal field (D_T) values, the total magnetizations of the three nano-Heusler compounds undergo a first order transition or second order transition (when increasing the parameter J_{Ru-X} value). Finally, the surface of the loops and the coercive field are important in the Ru_2MnTa compound followed by the Ru_2MnNb compound and less important in the Ru_2MnV one. Furthermore, when

increasing the exchange coupling parameter J_{Ru-X} , the coercive field and the surface of the loops also tends to increase.

References

- [1] W. Everhart and J. Newkirk, *Heliyon*, **5** (2019) e01578.
- [2] C. Felser and A. Hirohata, Eds., *Heusler Alloys*, Springer International Publishing, 2016.
- [3] G. Rogl, S. Ghosh, L. Wang, J. Bursik, A. Grytsiv, M. Kerber, E. Bauer, R. C. Mallik, X.Q. Chen, M. Zehetbauer and P. Rogl, *Acta Materialia*, **183** (2020) 285.
- [4] S. Idrissi, S. Ziti, H. Labrim, L. Bahmad, I. El Housni, R. Khalladi, S. Mtougui and N. El Mekkaoui, *Journal of Alloys and Compounds*, **820** (2020) 153373.
- [5] M. I. Khan, H. Arshad, M. Rizwan, S. S. A. Gillani, M. Zafar, S. Ahmed and M. Shakil, *Journal of Alloys and Compounds*, **819** (2020) 152964.
- [6] S. A. Khandy and J.D. Chai, *Journal of Applied Physics*, **127** (2020) 165102.
- [7] R. Djelti, A. Besbes and B. Bestani, *Optical and Quantum Electronics*, **52** (2020) 1.
- [8] Y. Zhang, W. Zhang, X. Yu, C. Yu, Z. Liu, G. Wu and F. Meng, *Materials Science and Engineering: B*, **260** (2020) 114654.
- [9] G. Forozani, A. A. Mohammad Abadi, S. M. Baizae and A. Gharaati, *Journal of Alloys and Compounds*, **815** (2020) 152449.
- [10] A. Ahmad, A.K. Das and S.K. Srivastava, *The European Physical Journal B*, **93** (2020) 1.
- [11] C. Felser, L. Wollmann, S. Chadov, G.H. Fecher and S.S.P. Parkin, *APL Materials*, **3** (2015) 041518.
- [12] S. A. Sofi and D. C. Gupta, *Journal of Solid State Chemistry*, **284** (2020) 121178.
- [13] F. Meng, S. Liu, K. Sun, R. Gao, X. Shi and H. Luo, *Journal of Magnetism and Magnetic Materials*, **514** (2020) 167161.
- [14] R. Murugeswari, M. Manikandan, R. Rajeswarapalanichamy and A. Milton Franklin Benial, *International Journal of Modern Physics B*, **34** (2020) 2050055.

- [15] M. Ram, A. Saxena, N. Limbu, H. Joshi and A. Shankar, *Journal of Applied Physics*, **128** (2020) 053901.
- [16] S. R. Hari, V. Srinivas, C. R. Li and Y. K. Kuo, *Journal of Physics: Condensed Matter*, **32** (2020) 355706.
- [17] Y. Gupta, M. M. Sinha and S. S. Verma, *Physica B: Condensed Matter*, **590** (2020) 412222.
- [18] M. Yang, W. Wang, B.C. Li, H.J. Wu, S.Q. Yang and J. Yang, *Physica A*, **539** (2020) 122932.
- [19] H.J. Wu, W. Wang, F. Wang, B.C. Li, Q and J.H. Xu, *Journal of Physics and Chemistry of Solids*, **136** (2020) 109174.
- [20] Z. Fadil, M. Qajjour, A. Mhirech, B. Kabouchi, L. Bahmad, and W. Ousi Benomar, *Ferroelectrics*, **573** (2021). In press.
- [21] Z. Fadil, A. Mhirech, B. Kabouchi, L. Bahmad, and W. Ousi Benomar, *Integrated Ferroelectrics*, **213** (2021). **In press.**
- [22] Z. Fadil, A. Mhirech, B. Kabouchi, L. Bahmad and W. Ousi Benomar, *Physics Letters A*, **384** (2020) 126783.
- [23] Z. Fadil, A. Mhirech, B. Kabouchi, L. Bahmad, and W. Ousi Benomar, *Superlattices and Microstructures*, **135** (2019) 106285.
- [24] R. Masrour and A. Jabar, *Physica A*, **539** (2020) 122878.
- [25] R. Masrour and A. Jabar, *Physica A*, **538** (2020) 122959.
- [26] I.J.L. Diaz and N.S. Branco, *Physica A*, **540** (2020) 123014.
- [27] Z. Fadil, N. Maaouni, A. Mhirech, B. Kabouchi, L. Bahmad and W. Ousi Benomar, *International Journal of Thermophysics*, (2021). **In press.**
- [28] Z. Fadil, A. Mhirech, B. Kabouchi, L. Bahmad and W. Ousi Benomar, *Chinese Journal of Physics*, **67** (2020) 123.
- [29] Z. Fadil, A. Mhirech, B. Kabouchi, L. Bahmad and W. Ousi Benomar, *Solid State Communications*, **316-317** (2020) 113944.

- [30] Z. Fadil, A. Mhirech, B. Kabouchi, L. Bahmad and W. Ousi Benomar, Superlattices and Microstructures, **134** (2019) 106224.
- [31] Z. Fadil, M. Qajjour, A. Mhirech, B. Kabouchi, L. Bahmad, and W. Ousi Benomar, Physica B: Condensed Matter, **564** (2019) 104.
- [32] S. Idrissi, S. Ziti, H. Labrim, R. Khalladi, S. Mtougui, N. El Mekkaoui, I. El Housni and L. Bahmad, Physica A: Statistical Mechanics and its Applications, **527** (2019) 121406.
- [33] V. V. Sokolovskiy, Y.A. Sokolovskaya, M.A. Zagrebin, V.D. Buchelnikov and A.T. Zayak, Journal of Magnetism and Magnetic Materials, **470** (2019) 64.
- [34] E. E. Smolyakova, M.A. Zagrebin., V.V. Sokolovskiy and V.D. Buchelnikov, Materials Today: Proceedings, **4** (2017) 4621.
- [35] V. V. Sokolovskiy, V. D. Buchelnikov, V. V. Khovaylo, S. V. Taskaev and P. Entel, International Journal of Refrigeration, **37** (2014) 273.
- [36] Idrissi, S., Labrim, H., Ziti, S., Bahmad, L., Physics Letters, Section A: General, Atomic and Solid State Physics, 2020, 384(24), 126453.
- [37] Idrissi, S., Ziti, S., Labrim, H., ...Mtougui, S., El Mekkaoui, N., Journal of Alloys and Compounds, 2020, 820, 153373.
- [38] Idrissi, S., Labrim, H., Ziti, S., Bahmad, L., Journal of Superconductivity and Novel Magnetism, 2020, 33(10), pp. 3087–3095.
- [39] Idrissi, S., Bahmad, L., Ziti, S., ...El Housni, I., Mtougui, S., Applied Physics A: Materials Science and Processing, 2019, 125(5), 306.